

The Lambda(1405) is a $\bar{K}N$ molecule

**Jonathan M. M. Hall^a, Waseem Kamleh^{*a†}, Derek B. Leinweber^a,
Benjamin J. Menadue^{a,b}, Benjamin J. Owen^a,
Anthony W. Thomas^{a,c}, Ross D. Young^{a,c}**

^a *Special Research Centre for the Subatomic Structure of Matter (CSSM),
Department of Physics, University of Adelaide, South Australia 5005, Australia*

^b *National Computational Infrastructure (NCI),
Australian National University, Australian Capital Territory 0200, Australia*

^c *ARC Centre of Excellence for Particle Physics at the Terascale (CoEPP),
Department of Physics, University of Adelaide, South Australia 5005, Australia*

E-mail: waseem.kamleh@adelaide.edu.au

We review recent lattice QCD results from the CSSM using the variational method to isolate the $\Lambda(1405)$ and explore its structure. The behaviour of the electric and magnetic form factors as the up and down quark masses approach their physical values, together with a Hamiltonian effective-field-theory model analysis of the lattice QCD energy levels, reveal that the structure is dominated by a bound antikaon-nucleon component [1].

The 8th International Workshop on Chiral Dynamics, CD2015

29 June 2015 - 03 July 2015

Pisa, Italy

*Speaker.

†We thank PACS-CS Collaboration for making their 2 + 1 flavor configurations available and acknowledge the ongoing support of the ILDG. This research was undertaken with the assistance of resources at the NCI National Facility in Canberra, Australia, and the iVEC facilities at Murdoch University (iVEC@Murdoch) and the University of Western Australia (iVEC@UWA). These resources are provided through the National Computational Merit Allocation Scheme and the University of Adelaide Partner Share supported by the Australian Government. We also acknowledge eResearch SA for their support of our supercomputers. This research is supported by the Australian Research Council through the ARC Centre of Excellence for Particle Physics at the Terascale, and through Grants DP150103164 (DBL), DP120104627 (DBL), DP140103067 (DBL and RDY), FT120100821 (RDY) and FL0992247 (AWT).

1. Introduction

The $J^P = 1/2^-$ ground-state resonance of the Λ baryon, the $\Lambda(1405)$, lies anomalously low in mass. At $1405.1_{-1.0}^{+1.3}$ MeV [2], it not only lies lower than the first positive-parity excited state, but also lower than the negative-parity ground state of the nucleon – even though it has a strange valence quark. Identifying the explanation for this observation has challenged theorists since its discovery in the 1960s [3]. While the quantum numbers of the $\Lambda(1405)$ can be described by three quarks, (uds), its totally unexpected position in the spectrum has rendered its structure quite mysterious.

Using the variational method, the CSSM presented results showing the isolation of the $\Lambda(1405)$ on the lattice [4] and a subsequent calculation of its electromagnetic form factors [1]. This calculation reveals the vanishing of the strange quark contribution to the magnetic form factor of the $\Lambda(1405)$ in the regime where the masses of the up and down quarks approach their physical values.

This result is very naturally explained if the state becomes a molecular $\bar{K}N$ bound state in that limit. In this case the strange quark is confined within a spin-0 kaon and has no preferred spin orientation. Because the anti-kaon has zero orbital angular momentum in order to conserve parity, the strange quark *cannot* contribute to the magnetic form factor of the $\Lambda(1405)$. On the other hand, if the $\Lambda(1405)$ were a $\pi\Sigma$ state or an elementary three-quark state the strange quark must make a sizable contribution to the magnetic form factor. Only if the $\bar{K}N$ component in the structure of the $\Lambda(1405)$ is dominant would one expect to find a vanishing strange-quark magnetic form factor.

In these proceedings we provide a review of the CSSM studies that led to this remarkable result, commencing with the variational method which is critical to isolating this state on the lattice.

2. Variational Analysis

To extract correlation functions from a variational analysis [5, 6, 7], we first need to construct the correlation matrix. If we consider some set of operators $\{\chi_i\}$ that couple to the states of interest, the associated correlation matrix can be written as

$$G_{ij}(\Gamma; \mathbf{p}; t) = \sum_{\mathbf{x}} e^{-i\mathbf{p}\cdot\mathbf{x}} \text{tr}(\Gamma \langle \Omega | \chi_i(x) \bar{\chi}_j(0) | \Omega \rangle), \quad (2.1)$$

where Γ is some Dirac matrix that sensibly selects the appropriate components of the resultant spinor matrix. We then solve for the left ($\mathbf{v}^\alpha(\mathbf{p})$) and right ($\mathbf{u}^\alpha(\mathbf{p})$) generalised eigenvectors of $G(\Gamma; \mathbf{p}; t + \delta t)$ and $G(\Gamma; \mathbf{p}; t)$, so that

$$G(\Gamma; \mathbf{p}; t + \delta t) \mathbf{u}^\alpha(\mathbf{p}) = e^{-E_\alpha(\mathbf{p}) \delta t} G(\Gamma; \mathbf{p}; t) \mathbf{u}^\alpha(\mathbf{p}), \text{ and} \quad (2.2)$$

$$\mathbf{v}^{\alpha\top}(\mathbf{p}) G(\Gamma; \mathbf{p}; t + \delta t) = e^{-E_\alpha(\mathbf{p}) \delta t} \mathbf{v}^{\alpha\top}(\mathbf{p}) G(\Gamma; \mathbf{p}; t). \quad (2.3)$$

These eigenvectors identify the “ideal” combinations ϕ^α of the original operators χ_i that perfectly isolate individual energy eigenstates at momentum \mathbf{p} . As such, we can write

$$\phi^\alpha(\mathbf{p}) = v_i^\alpha(\mathbf{p}) \chi_i \quad \bar{\phi}^\alpha(\mathbf{p}) = \bar{\chi}_i u_i^\alpha(\mathbf{p}). \quad (2.4)$$

Note that the Greek indices, α and β , label states and are not to be summed when repeated. Using these operators, we can construct the eigenstate-projected correlation functions for the individual

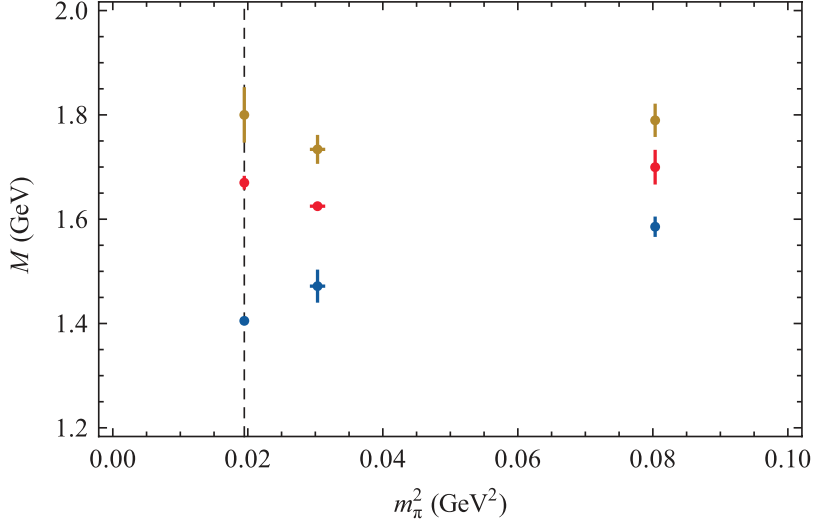


Figure 1: The lowest-lying eigenstate-projected masses using SU(3)-flavour-symmetry-specific operators χ^1 , χ_1^8 , and χ_2^8 plotted against m_π^2 . Using these operators allows us to isolate three low-lying states.

states,

$$G_\alpha(\Gamma; \mathbf{p}; t) = \mathbf{v}^{\alpha\top}(\mathbf{p}) G(\Gamma; \mathbf{p}; t) \mathbf{u}^\alpha(\mathbf{p}), \quad (2.5)$$

which may then be analysed using standard lattice techniques. By fitting a single state ansatz to the eigenstate-projected effective energies we are able to obtain robust values for the excited state energy spectrum [8].

As the $\Lambda(1405)$ has the valence quark assignment of (u, d, s) , it has overlap with both octet and singlet flavour symmetries. The flavour symmetry is exact when all three quarks have the same mass and electromagnetic charges are neglected. However, the strange quark mass is much larger than the u and d quark masses, and one expects that the eigenstates of QCD should involve a superposition of octet and singlet symmetries. We consider local three-quark operators providing both scalar and vector diquark spin configurations for the quarks [9],

$$\chi_1^8 = \frac{1}{\sqrt{6}} \varepsilon^{abc} \left(2(u^a C \gamma_5 d^b) s^c + (u^a C \gamma_5 s^b) d^c - (d^a C \gamma_5 s^b) u^c \right), \quad (2.6)$$

$$\chi_2^8 = \frac{1}{\sqrt{6}} \varepsilon^{abc} \left(2(u^a C d^b) \gamma_5 s^c + (u^a C s^b) \gamma_5 d^c - (d^a C s^b) \gamma_5 u^c \right), \quad (2.7)$$

$$\chi^1 = 2\varepsilon^{abc} \left((u^a C \gamma_5 d^b) s^c - (u^a C \gamma_5 s^b) d^c + (d^a C \gamma_5 s^b) u^c \right), \quad (2.8)$$

where we have suppressed the spacetime coordinate dependence for clarity. Note that in the flavour-singlet case, the two Dirac structures are related through a Fierz transformation.

We also expand our operator basis by including operators smeared by differing amounts of gauge-invariant Gaussian smearing [10]. Our analysis is based on a 6×6 correlation matrix formed by using the flavour-octet operators χ_1^8 , χ_2^8 , and the flavour-singlet operator χ^1 together with 16 and 100 sweeps of smearing.

The quark-mass dependence of the lowest lying states observed in our lattice QCD calculations [4] is illustrated in Fig. 1 at each of the pion masses available in the PACS-CS simulations.

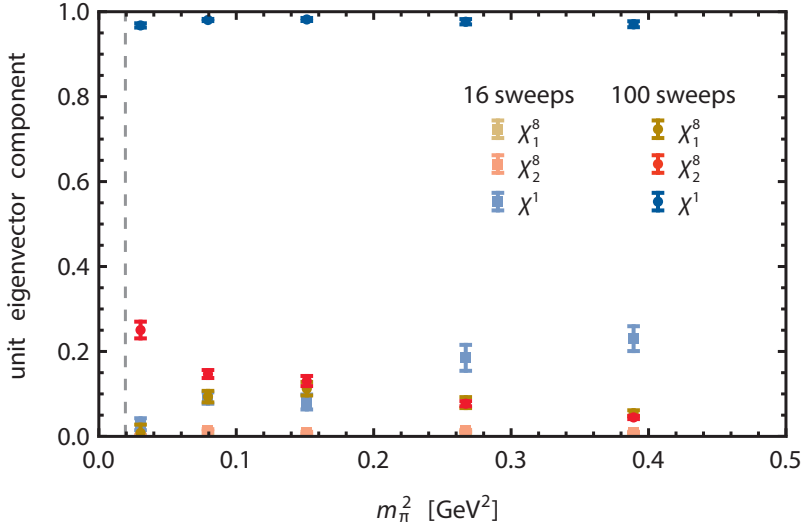


Figure 2: Relative strength of each interpolating field’s eigenvector component, $u_i(\mathbf{0})$ of Eq. (2.4), for the $\Lambda(1405)$ as a function of m_π^2 . The light-coloured points are smeared with 16 sweeps of smearing and the dark points with 100 sweeps. The gold points correspond to the flavour-octet operator with a $(qC\gamma_5 q)q$ Dirac structure, the red points correspond to the same flavour-octet structure but with a $(qCq)\gamma_5 q$ Dirac structure. The blue points correspond to the flavour-singlet operator.

The mixing of spin-flavour symmetries in the QCD eigenstates demands a linear superposition of these interpolators when creating an eigenstate of QCD. The correlation matrix approach provides an effective means for determining this superposition. The lowest state observed, corresponding to the $\Lambda(1405)$, is singlet-dominated whereas the two higher excited states are octet-dominated.

Figure 2 displays the flavour composition of the $\Lambda(1405)$ in the relative components of the different interpolating fields from a 6×6 correlation matrix as the pion-mass varies. While the highly-smeared, flavour-singlet operator is always the dominant contribution, an octet component becomes important away from the $SU(3)$ -flavour-symmetry limit. A comparison of the energy of the $\Lambda(1405)$ with a single unit of lattice momentum and the dispersion relation $\sqrt{m^2 + \mathbf{p}^2}$ is shown in Figure 3.

3. Electromagnetic Form Factors

The isolation of an individual energy eigenstate enables the investigation of other properties of the $\Lambda(1405)$ on the finite volume lattice. The electromagnetic form factors are particularly interesting as they provide insight into the distribution of charge and magnetism within the $\Lambda(1405)$. Moreover, the form factors can be resolved one quark flavour at a time.

To measure the electromagnetic properties of the $\Lambda(1405)$ in Lattice QCD, one probes the state with the conserved vector current carrying three-momentum \vec{q} , at a time well separated from the creation and annihilation points to ensure single-state isolation. By taking the ratio of this three-point correlation function with the two-point correlation function from the mass-analysis, we create a direct measure of the Sachs electric and magnetic form factors. For an energy eigenstate

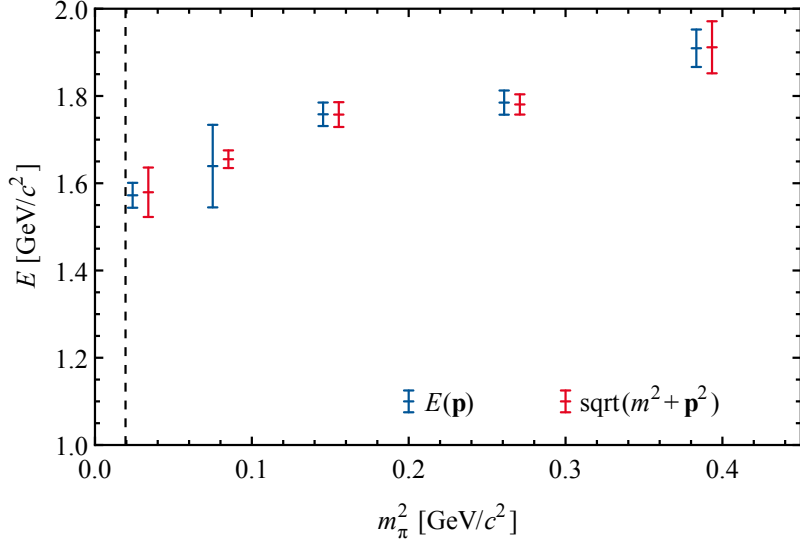


Figure 3: A plot of the energy of the $\Lambda(1405)$ with a single unit of lattice momentum as a function of m_π^2 , compared with the value expected from the dispersion relation $\sqrt{m^2 + \mathbf{p}^2}$.

α , the three-point correlation function is given by

$$G_\alpha^\mu(\Gamma; \mathbf{p}', \mathbf{p}; t_2, t_1) = \sum_{\mathbf{x}_1, \mathbf{x}_2} e^{-i\mathbf{p}' \cdot \mathbf{x}_2} e^{i(\mathbf{p}' - \mathbf{p}) \cdot \mathbf{x}_1} \text{tr}(\Gamma \langle \Omega | \phi^\alpha(x_2) j^\mu(x_1) \bar{\phi}^\alpha(0) | \Omega \rangle). \quad (3.1)$$

where j^μ is the current. We can rewrite this in the following form

$$G_\alpha^\mu(\Gamma; \mathbf{p}', \mathbf{p}; t_2, t_1) = e^{-E_\alpha(\mathbf{p}')(t_2 - t_1)} e^{-E_\alpha(\mathbf{p})t_1} \text{tr} \left(\Gamma \sum_{s, s'} \langle \Omega | \phi^\alpha | p', s' \rangle \langle p', s' | j^\mu | p, s \rangle \langle p, s | \bar{\phi}^\alpha | \Omega \rangle \right) \quad (3.2)$$

in order to extract the current matrix element $\langle p', s' | j^\mu | p, s \rangle$ that encodes the form factors of the interaction.

Using the nature of the optimal operators ϕ^α , we can define the ideal three-point correlation function in terms of the non-projected three-point correlation functions G_{ij}^μ as

$$G_\alpha^\mu(\Gamma; \mathbf{p}', \mathbf{p}; t_2, t_1) = \mathbf{v}^{\alpha\top}(\mathbf{p}') G^\mu(\Gamma; \mathbf{p}', \mathbf{p}; t_2, t_1) \mathbf{u}^\alpha(\mathbf{p}). \quad (3.3)$$

To eliminate the temporal dependence of the three-point correlation function, we construct the following ratio of three- and two-point functions [9, 11]

$$R_\alpha^\mu(\Gamma', \Gamma; \mathbf{p}', \mathbf{p}; t_2, t_1) = \left(\frac{G_\alpha^\mu(\Gamma; \mathbf{p}', \mathbf{p}; t_2, t_1) G_\alpha^\mu(\Gamma; \mathbf{p}, \mathbf{p}'; t_2, t_1)}{G_\alpha(\Gamma'; \mathbf{p}'; t_2) G_\alpha(\Gamma'; \mathbf{p}; t_2)} \right)^{1/2}. \quad (3.4)$$

The current matrix element for spin-1/2 baryons can be written in the form

$$\langle p', s' | j^\mu | p, s \rangle = \left(\frac{m_\alpha^2}{E_\alpha(\mathbf{p}) E_\alpha(\mathbf{p}')} \right)^{1/2} \bar{u} \left(F_1(q^2) \gamma^\mu + i F_2(q^2) \sigma^{\mu\nu} \frac{q^\nu}{2m_\alpha} \right) u, \quad (3.5)$$

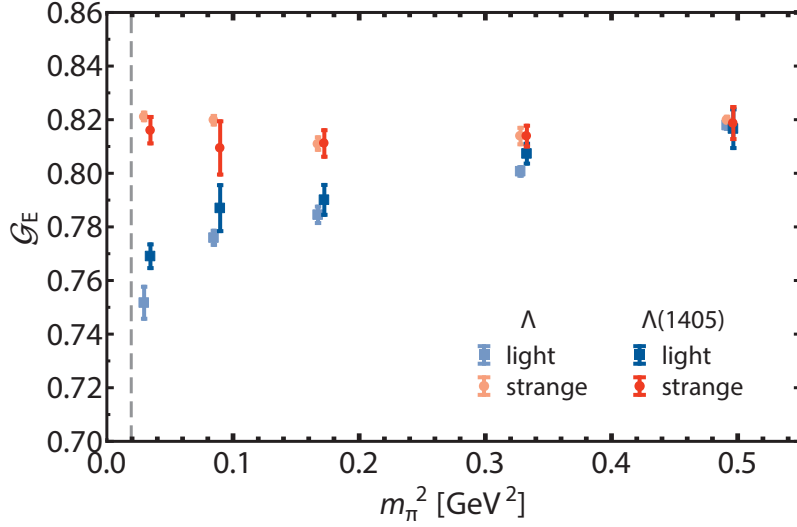


Figure 4: Sachs electric form factors at $Q^2 = 0.16 \text{ GeV}^2/c^2$. Results for the individual unit-charged quark flavour sectors for the $\Lambda(1405)$ (dark points) are compared with those for the ground state Λ (light).

where F_1 and F_2 are the Dirac and Pauli form factors. These are related to the Sachs form factors through

$$\mathcal{G}_E(q^2) = F_1(q^2) - \frac{q^2}{(2m_\alpha)^2} F_2(q^2), \text{ and} \quad (3.6)$$

$$\mathcal{G}_M(q^2) = F_1(q^2) + F_2(q^2). \quad (3.7)$$

A suitable choice of momentum \mathbf{q} and the Dirac matrices Γ and Γ' allows us to directly access the Sachs electric and magnetic form factors through an “effective” lattice form factor [9], with further technical details of the extraction technique provided elsewhere [12].

Figure 4 presents the pion mass dependence of the Sachs electric form factors for the individual quark sectors for both the $\Lambda(1405)$ and the ground-state even-parity Λ at $Q^2 = 0.16 \text{ GeV}^2/c^2$. We see little change between the ground state Λ and the $\Lambda(1405)$. At heavy quark masses approaching the flavour-symmetry limit, the light (u or d) quarks in the $\Lambda(1405)$ have the same distribution as the strange quark as required by the singlet symmetry. As the u and d quarks become light, we observe a significant departure from the flavour symmetry, reminiscent of Fig. 2 where the octet interpolator becomes important for the excitation of the $\Lambda(1405)$ in the light-quark region. It is also interesting to note that the strange quark form factor variation is a pure environmental effect as the mass of the strange quark is held fixed.

The deviation from this flavour-singlet picture as the pion mass approaches its physical value is consistent with the development of a $\bar{K}N$ component in the structure of the $\Lambda(1405)$. If we consider such a dressing, the centre of mass lies nearer the heavier nucleon, so the anti-light-quark contribution is distributed further out by the \bar{K} ; this yields an enhanced light-quark form factor. Similarly, the strange quark is also distributed further out by the \bar{K} and this results in a suppressed form factor relative to the ground state Λ .

The strange quark magnetic form factor of the $\Lambda(1405)$ is crucial to the present analysis because it provides direct insight into the possible dominance of a molecular $\bar{K}N$ bound state. In

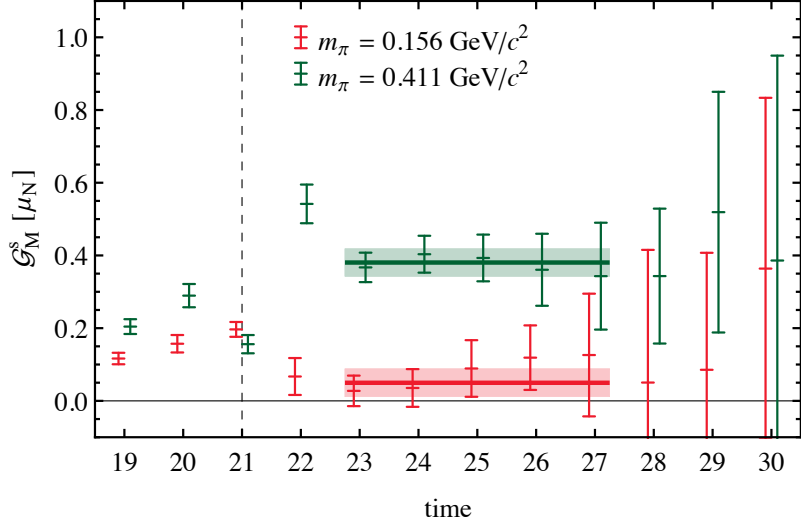


Figure 5: Ratio of three- and two-point functions providing the strange-quark contribution to the Sachs magnetic form factor of the $\Lambda(1405)$ at $Q^2 \simeq 0.16 \text{ GeV}^2/c^2$. Results at two different pion masses describing the light u and d quark masses are illustrated. The vertical dashed line indicates the introduction of the electromagnetic current at $t = 21$ following the baryon source at $t = 16$.

forming such a molecular state, the $\Lambda(u, d, s)$ valence quark configuration is complemented by a u, \bar{u} quark–anti-quark pair making a $K^-(s, \bar{u})$ proton (u, u, d) bound state, or a d, \bar{d} quark–anti-quark pair making a $\bar{K}^0(s, \bar{d})$ neutron (d, d, u) bound state. In both cases the strange quark is confined within a spin-0 kaon and has no preferred spin orientation. Because of this and the fact that the anti-kaon has zero orbital momentum in order to conserve parity, the strange quark *cannot* contribute to the magnetic form factor of the $\Lambda(1405)$. On the other hand, if the $\Lambda(1405)$ were a $\pi\Sigma$ state or an elementary three-quark state the strange quark must make a sizable contribution to the magnetic form factor. In summary, only if the $\bar{K}N$ component in the structure of the $\Lambda(1405)$ is dominant would one expect to find a vanishing strange quark magnetic form factor.

Figure 5 presents the Euclidean time dependence of the three- and two-point correlation function ratio for the strange quark contribution to the Sachs magnetic form factor, \mathcal{G}_M^s , of the $\Lambda(1405)$ at $Q^2 \simeq 0.16 \text{ GeV}^2/c^2$. Results for two different ensembles are presented. As is standard for quark-sector contributions, the electric charge factor for the quark charge has not been included; *i.e.* the result is for a single quark of unit charge. The best fit plateaus, as identified by a covariance matrix based χ^2 analysis, are also illustrated. The rapid onset of the plateau following the electromagnetic current at $t = 21$ reflects our use of optimised interpolating fields.

Figure 6 presents \mathcal{G}_M^s for the $\Lambda(1405)$ at $Q^2 \simeq 0.16 \text{ GeV}^2/c^2$ for all five ensembles available from PACS-CS. Variation of the light u and d quark masses is indicated by the squared pion mass, m_π^2 . At the heaviest u and d quark masses approaching the $SU(3)$ flavour limit, $m_u = m_d = m_s$, the underlying approximate flavour-singlet structure is manifest in \mathcal{G}_M^s with the light and strange sectors contributing equally. Even though the light-quark sector is becoming much lighter, this symmetry persists well towards the physical point. Only by directly simulating QCD in the realm of quark masses realised in Nature can the vanishing of the strange quark contribution be revealed.

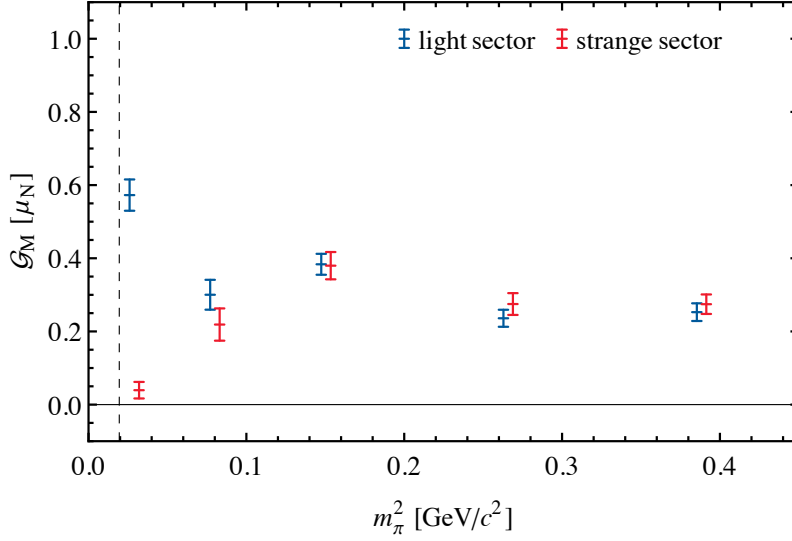


Figure 6: The light (u or d) and strange (s) quark contributions to the magnetic form factor of the $\Lambda(1405)$ at $Q^2 \simeq 0.16$ GeV^2/c^2 are presented as a function of the light u and d quark masses, indicated by the squared pion mass, m_π^2 . Sector contributions are for single quarks of unit charge. The vertical dashed line indicates the physical pion mass.

At the lightest quark-mass ensemble closest to Nature, the strange quark contribution to the magnetic form factor of the $\Lambda(1405)$ drops by an order of magnitude and approaches zero. As the simulation parameters describing the strange quark are held fixed, this is a remarkable environmental effect of unprecedented strength. As the u and d quark masses become light, and the cost of creating u, \bar{u} and d, \bar{d} quark–anti-quark pairs from the QCD vacuum diminishes, we observe an important rearrangement of the quark structure within the $\Lambda(1405)$ consistent with the dominance of a molecular $\bar{K}N$ bound state.

4. Hamiltonian Model

To connect these results obtained for a QCD eigenstate on the finite volume of the lattice to the infinite volume baryon resonance of Nature, we construct a finite-volume Hamiltonian model using a basis of single- and two-particle non-interacting meson-baryon states available on the finite-volume periodic lattice. We follow the approach established in Ref. [13] where the eigenvalue equation of the model is designed to reproduce finite-volume chiral effective field theory [14, 15, 16, 17] in the weak coupling limit. Finite-volume models [13, 18] are particularly useful in interpreting the composition of the energy spectrum observed in Lattice QCD simulations.

In constructing the Hamiltonian, the four octet meson-baryon interaction channels of the $\Lambda(1405)$ are included [19]: $\pi\Sigma$, $\bar{K}N$, $K\Xi$, $\eta\Lambda$. We begin by writing the Hamiltonian H as the sum of free and interacting Hamiltonians, $H = H_0 + H_I$. The rows and columns of H represent the magnitudes of the three-momenta available to the meson-baryon intermediate states dressing the bare $\Lambda(1405)$ state. As we work with total momentum zero, the meson and the baryon will each carry the same magnitude of momentum in a back-to-back orientation. In a finite periodic volume, momentum is quantised. Working on a cubic volume of extent L on each side, it is convenient to

define the momentum magnitudes

$$k_n = \sqrt{n_x^2 + n_y^2 + n_z^2} \frac{2\pi}{L}, \quad (4.1)$$

with $n_i = 0, 1, 2, \dots$ and integer $n = n_x^2 + n_y^2 + n_z^2$. As there are permutations of the n_i that give rise to the same momentum magnitude, we also introduce the integer $C_3(n)$ as a combinatorial factor equal to the number of unique permutations of $\pm n_x, \pm n_y$ and $\pm n_z$. For example, the lowest lying nontrivial momentum available on the lattice, where one direction has the magnitude of $2\pi/L$, has $C_3(1) = 6$. The result recognises three positions for the non-trivial momentum and a factor of two associated with whether the meson or the baryon carries the positive momentum.

The non-interacting Hamiltonian H_0 has diagonal entries corresponding to the relativistic non-interacting meson-baryon energies available on the finite periodic volume at total three-momentum zero. It also includes a single-particle state with bare mass, $m_0 + \alpha_0 m_\pi^2$. The parameters m_0 and α_0 are to be constrained by the lattice QCD results. Denoting each meson-baryon energy by $\omega_{MB}(k_n) = \omega_M(k_n) + \omega_B(k_n)$, with $\omega_A(k_n) \equiv \sqrt{k_n^2 + m_A^2}$, the non-interacting Hamiltonian takes the form

$$H_0 = \begin{pmatrix} m_0 + \alpha_0 m_\pi^2 & 0 & 0 & \dots \\ & \omega_{\pi\Sigma}(k_0) & & \\ 0 & & \ddots & 0 & \dots \\ & & & \omega_{\eta\Lambda}(k_0) & \\ & & & & \omega_{\pi\Sigma}(k_1) & \\ 0 & 0 & & & & \ddots & \dots \\ & & & & & & \omega_{\eta\Lambda}(k_1) & \\ \vdots & \ddots \end{pmatrix}. \quad (4.2)$$

In the present model the interaction entries describe the coupling of the single-particle state to the two-particle meson-baryon states.

$$H_I = \begin{pmatrix} 0 & g_{\pi\Sigma}(k_0) & \dots & g_{\eta\Lambda}(k_0) & g_{\pi\Sigma}(k_1) & \dots & g_{\eta\Lambda}(k_1) & \dots \\ g_{\pi\Sigma}(k_0) & 0 & \dots & & & & & \\ \vdots & \vdots & 0 & & & & & \\ g_{\eta\Lambda}(k_0) & & & \ddots & & & & \\ g_{\pi\Sigma}(k_1) & & & & \ddots & & & \\ \vdots & & & & & \ddots & & \\ g_{\eta\Lambda}(k_1) & & & & & & \ddots & \\ \vdots & & & & & & & \ddots \end{pmatrix}. \quad (4.3)$$

Each entry represents the S -wave interaction energy of the $\Lambda(1405)$ with one of the four channels at a certain value for k_n . The form of the interaction is derived from effective field theory, and includes the relevant finite-volume factors [13]

$$g_{MB}(k_n) = \left(\frac{\kappa_{MB}}{16\pi^2 f_\pi^2} \frac{C_3(n)}{4\pi} \left(\frac{2\pi}{L} \right)^3 \omega_M(k_n) u^2(k_n) \right)^{1/2}. \quad (4.4)$$

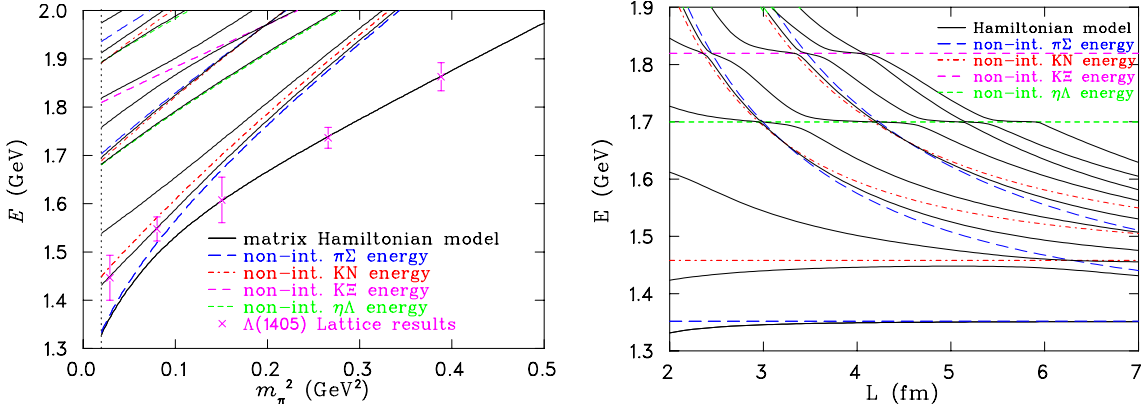


Figure 7: (left) The quark-mass dependence ($m_q \propto m_\pi^2$) of the lowest-lying $\Lambda(1405)$ states observed in our lattice QCD calculations [1] is illustrated by the discrete points at each of the pion masses available in the PACS-CS ensembles. The low-lying energy spectrum of our Hamiltonian model (solid curves) constrained to the Lattice QCD results (discrete points) is also illustrated. The associated non-interacting meson-baryon basis states are illustrated by the dashed curves. **(right)** The volume dependence of the spin-1/2 odd-parity Λ spectrum obtained from our Hamiltonian effective field theory analysis of our lattice results at $m_\pi = 156$ MeV. L denotes the length of the L^3 volume.

$f_\pi = 92.4$ MeV represents the pion decay constant and $u^2(k_n)$ is a regulator function. For the purposes of this model, $u(k_n)$ takes the form of a dipole regulator, with a regularization scale of $\Lambda = 0.8$ GeV. It has been shown in previous investigations that the regulator dependence is small in the extraction of resonance parameters near the physical pion mass [20]. The coupling κ_{MB} is related to the $SU(3)$ -flavour singlet couplings of the octet mesons and baryons via [21, 22]

$$\kappa_{\pi\Sigma} = 3\xi_0, \quad \kappa_{\bar{K}N} = 2\xi_0, \quad \kappa_{K\xi} = 2\xi_0, \quad \kappa_{\eta\Lambda} = \xi_0, \quad (4.5)$$

with $\xi_0 = 0.75$, chosen in order to ensure that the $\pi\Sigma$ decay width of the $\Lambda(1405)$ takes the physical value of 50 ± 2 MeV [23] at the physical pion mass, in the infinite-volume limit.

The eigenvalue equation corresponding to the Hamiltonian model presented here takes the following simple form which is similar to chiral effective field theory in a finite volume,

$$\lambda = m_0 + \alpha_0 m_\pi^2 - \sum_{M,B} \sum_{n=0}^{\infty} \frac{g_{MB}^2(k_n)}{\omega_{MB}(k_n) - \lambda}. \quad (4.6)$$

M and B denote the intermediate meson-baryon pairs, with coupling $g_{MB}(k_n)$ provided in Eq. (4.4). λ is the energy eigenvalue of the S -wave interaction, which occurs on both sides of the equation. As λ is finite, the pole in the denominator of the right-hand side is never accessed. A nontrivial mixing of states occurs and the bare mass $m_0 + \alpha_0 m_\pi^2$ encounters self-energy corrections that lead to avoided level-crossings in the finite-volume energy eigenstates.

To solve this Hamiltonian system, the *dgeev* routine from the LAPACK software library is used to obtain the eigenvalues and eigenvectors of H . The energy eigenvalues of the matrix may be fitted to their corresponding lattice QCD values by minimising the chi-square function for the parameters m_0 and α_0 at different values of m_π^2 . The low-lying energy eigenvalues fit to the lattice QCD results are illustrated in Fig. 7. The scale is set via the Sommer parameter [24].

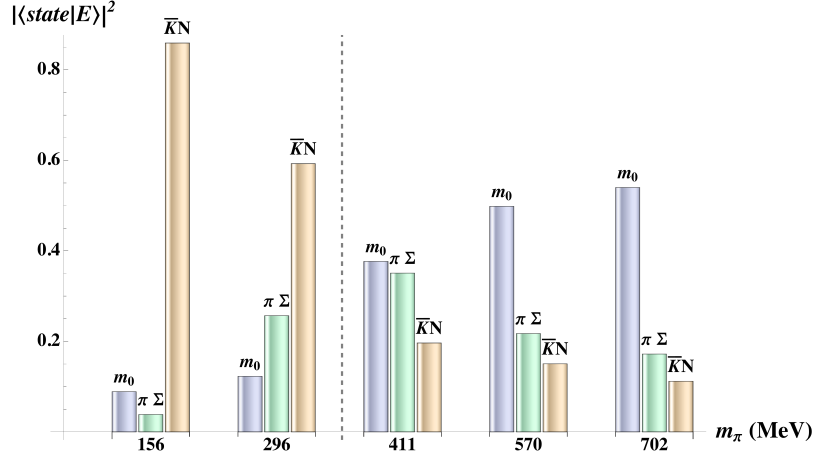


Figure 8: The overlap of the basis state, $|state\rangle$, with the energy eigenstate $|E\rangle$, illustrating the composition of the states associated with the lattice simulation results. Basis states include the single particle (bare three-quark) state, denoted by m_0 , and the two-particle states $\pi\Sigma$ and $\bar{K}N$. A sum over all two-particle momentum states is done in reporting the probability for the two-particle channels. Pion masses are indicated on the x -axis with the vertical dashed line separating the first state for the heaviest three masses from the second state for the lightest two masses.

The states observed on the lattice are described very well by the Hamiltonian model. The three heaviest quark masses considered on the lattice correspond to a stable odd-parity $\Lambda(1405)$, as the $\pi\Sigma$ threshold energy exceeds that of the $\Lambda(1405)$. However, as the physical pion mass is approached, the $\pi\Sigma$ threshold energy decreases and a nontrivial mixing of states associated with an avoided level crossing of the transitioning $\pi\Sigma$ threshold occurs. At the lightest two quark masses considered, the $\Lambda(1405)$ corresponds to the second state of the Hamiltonian model with a $\pi\Sigma$ -dominated eigenstate occupying the lowest energy position. The reason this lowest-lying state is not seen on the lattice will become more apparent as the composition of the finite-volume eigenstates is examined.

The eigenvectors of the Hamiltonian system provide the overlap of the basis states with the eigenstates and thus describe the underlying composition of the eigenstates. As the first and second eigenstates are dominated by the single-particle state and the two-particle channels $\pi\Sigma$ and $\bar{K}N$, we illustrate these in Fig. 8 for each value of pion mass considered in the Lattice QCD simulations. A sum over all two-particle momentum states is done in reporting the probability of the two-particle channels.

At the lightest pion mass, $m_\pi = 156$ MeV, the second eigenstate in the Hamiltonian model is dominated by the $\bar{K}N$ channel in complete agreement with the explanation of the observed, vanishing strange quark contribution to the magnetic form factor. A small but nontrivial role for the single-particle three-quark state enables the excitation of this state in the lattice correlation matrix analysis of three-quark operators.

In contrast, the lowest-lying eigenstate of the Hamiltonian model at $m_\pi = 156$ MeV is dominated by $\pi\Sigma$, with very small single-particle content, which explains why it is missing from the lattice QCD spectrum. Similarly, the contribution from the single-particle state at the second pion

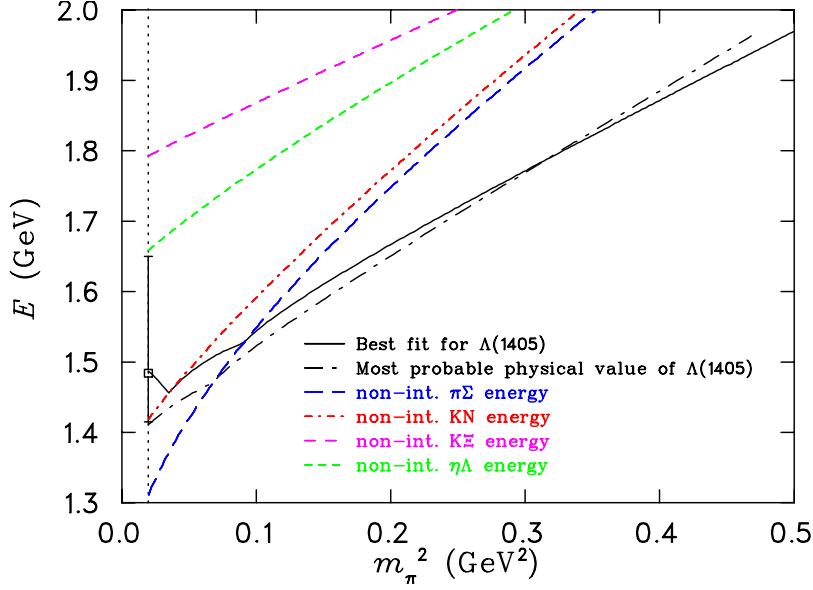


Figure 9: The quark mass dependence of the infinite-volume reconstruction of the $\Lambda(1405)$ energy is illustrated as a function of the squared pion-mass, m_π^2 . Both the fit to the central values of the lattice QCD results and the most probable mass dependence observed in the bootstrap ensemble analysis of the lattice results are illustrated.

mass is larger in the second state than in the first state. At the larger three pion masses, the single-particle state takes on a more important role, but significant two-particle mixing remains.

5. Infinite-Volume Limit

Having confirmed that the $\Lambda(1405)$ state observed on the lattice is best described as a molecular $\bar{K}N$ bound state, it remains to demonstrate the connection between the finite-volume lattice eigenstates and the infinite-volume resonance found in Nature. The quark-mass behaviour of the $\Lambda(1405)$ energy in the infinite-volume limit can be reconstructed from the finite-volume Hamiltonian model by considering the principal-value continuum versions of the loop integral contributions from all channels with the appropriate physical hadron masses. The resonance energy of the $\Lambda(1405)$ in infinite volume is

$$E_{\Lambda 1405} = m_0^{\text{fit}} + \alpha_0^{\text{fit}} m_\pi^2 + \sum_{M,B} \frac{\kappa_{MB}}{16\pi^2 f_\pi^2} \mathcal{P} \int_0^\infty dk \frac{k^2 \omega_M(k) u^2(k)}{E_{\Lambda 1405} - \omega_{MB}(k)}, \quad (5.1)$$

where \mathcal{P} indicates that the principal value integral is performed. This integral represents the infinite-volume version of the loop sum appearing in Eq. (4.6). Since $E_{\Lambda 1405}$ appears on both sides of Eq. (5.1), it is best solved iteratively by scanning over a range of possible values of $E_{\Lambda 1405}$.

The result is shown in Fig. 9 as a solid black line. The dashed lines illustrate the non-interacting infinite-volume S -wave threshold energies, which each induce a non-analytic cusp in the quark-mass dependence of the self energy.

To obtain an estimate of the statistical uncertainty in the $\Lambda(1405)$ energy, a bootstrap analysis is performed. This is achieved by repeating the minimisation of the chi-square to obtain fitted values

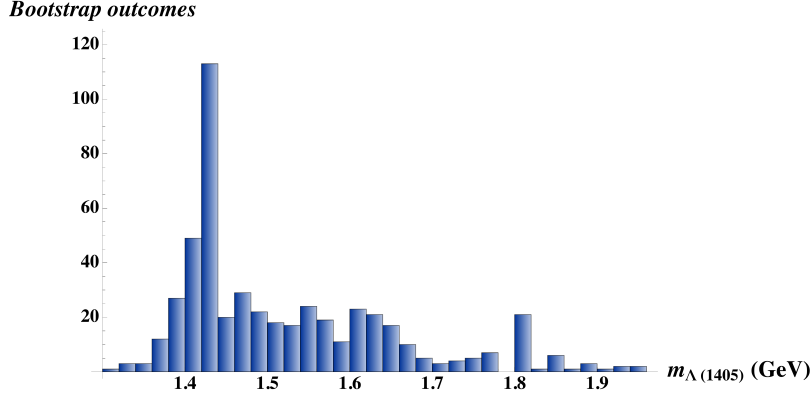


Figure 10: The statistical distribution of the infinite-volume $\Lambda(1405)$ resonance energy at the physical pion mass obtained from a bootstrap analysis of the Lattice QCD results.

of m_0 and α_0 for separate bootstrap ensembles of lattice QCD data. The bootstraps are calculated by altering the value of each lattice data point by a Gaussian-distributed random number, weighted by the uncertainty at each point in m_π^2 . The statistical distribution of values for the $\Lambda(1405)$ mass at the physical pion mass and infinite volume, for 500 bootstrap configurations, is shown in the form of a histogram, displayed in Fig. 10. The plot has an unconventional distribution due to cusps in the extrapolation associated with the opening of decay channel(s). The bootstrap error analysis provides a resonance energy of $1.48^{+0.17}_{-0.07}$ GeV.

The distribution of the bootstrap analysis is sharply peaked around the most probable value of 1.41 GeV in good agreement with experiment. We illustrate the most probable outcome for the $\Lambda(1405)$ mass dependence by the dot-dash curve in Fig. 9 labeled “Most probable physical value of $\Lambda(1405)$.” In this case only the $\pi\Sigma$ threshold induces a cusp and the ordering of the $\pi\Sigma$ threshold, the $\Lambda(1405)$ energy, and the $\bar{K}N$ threshold realised in Nature is reproduced.

6. Conclusion

First-principles lattice QCD calculations are complemented with Hamiltonian effective field theory, founded on the principles of finite-volume chiral perturbation theory, to study the quark-mass and volume dependence of the low-lying odd-parity states associated with the $\Lambda(1405)$. The $\Lambda(1405)$ has been identified on the lattice through a study of its quark mass dependence and its relation to avoided level crossings in effective field theory.

A variational analysis is performed to calculate the Sachs electric and magnetic form factors. The connected light-quark contribution to the $\Lambda(1405)$ has been investigated and shown to be consistent with $(\bar{K}^0 n$ and $K^- p)$ dressings of the nucleon. The vanishing of the strange quark contribution to the magnetic moment of the $\Lambda(1405)$ and the dominance of the $\bar{K}N$ component found in the finite-volume Hamiltonian effective field theory treatment reveal that the structure of the $\Lambda(1405)$ is dominated by a molecular bound state of an anti-kaon and a nucleon.

In the infinite-volume limit, the Hamiltonian model describes a quark mass dependence that is consistent with Nature. The connection between the continuum, infinite-volume pole positions and the finite-volume lattice energy levels is non-trivial. Studies of experimental results have suggested

the possibility of a double-pole structure in the 1400 MeV region of the Λ channel [25, 26, 27, 28, 29]. An independent Unitary- χPT analysis indicates our lattice data is consistent with a double-pole model where the $\Lambda(1405)$ is a dynamically generated resonance [30].

The resolution of the interacting scattering threshold energy levels on the lattice may provide further insight into the pole structure in the infinite-volume. This requires an expansion of the operator basis used in our correlation matrix as the coupling of local three-quark operators to multi-particle scattering states on the lattice is suppressed by the volume. Importantly, the presence of a nontrivial single-particle three-quark component in the Hamiltonian model eigenstate explains why our $\Lambda(1405)$ state is readily accessible in lattice correlation matrix analyses constructed with three-quark operators.

Due to the dominance of the flavour-singlet interpolator in forming the $\Lambda(1405)$ on the lattice, the Hamiltonian model presented here only considers the EFT flavour-singlet couplings. While the most important physics has been explained, one could also consider the addition of flavour-octet contributions. The inclusion of these octet contributions will likely prove important in the analysis of an expanded lattice spectrum that includes the interacting scattering thresholds, and this will be the subject of future work. Furthermore, one could also investigate the influence of coupling the current operator to the extended multi-hadron channels [31].

References

- [1] J. M. M. Hall, W. Kamleh, D. B. Leinweber, B. J. Menadue, B. J. Owen, A. W. Thomas, and R. D. Young, *Phys. Rev. Lett.* **114** (2015), no. 13 132002, [[arXiv:1411.3402](#)].
- [2] **Particle Data Group** Collaboration, K. Nakamura et al., *J. Phys.* **G37** (2010) 075021.
- [3] A. Engler, H. Fisk, R. Kraemer, C. Meltzer, and J. Westgard, *Phys. Rev. Lett.* **15** (1965) 224.
- [4] B. J. Menadue, W. Kamleh, D. B. Leinweber, and M. S. Mahbub, *Phys. Rev. Lett.* **108** (2012) 112001, [[arXiv:1109.6716](#)].
- [5] C. Michael, *Nucl. Phys.* **B259** (1985) 58.
- [6] M. Luscher and U. Wolff, *Nucl. Phys.* **B339** (1990) 222–252.
- [7] D. B. Leinweber, W. Melnitchouk, D. G. Richards, A. G. Williams, and J. M. Zanotti, *Lect. Notes Phys.* **663** (2005) 71–112, [[nucl-th/0406032](#)].
- [8] A. L. Kiratidis, W. Kamleh, D. B. Leinweber, and B. J. Owen, *Phys. Rev.* **D91** (2015) 094509, [[arXiv:1501.0766](#)].
- [9] D. B. Leinweber, R. Woloshyn, and T. Draper, *Phys. Rev.* **D43** (1991) 1659–1678.
- [10] S. Gusken, *Nucl. Phys. Proc. Suppl.* **17** (1990) 361–364.
- [11] S. Boinepalli, D. Leinweber, A. Williams, J. Zanotti, and J. Zhang, *Phys. Rev.* **D74** (2006) 093005, [[hep-lat/0604022](#)].
- [12] B. J. Menadue, W. Kamleh, D. B. Leinweber, M. S. Mahbub, and B. J. Owen, *PoS LATTICE2012* (2012) 178.
- [13] J. Hall, A. C. P. Hsu, D. Leinweber, A. Thomas, and R. Young, *Phys. Rev.* **D87** (2013) 094510, [[arXiv:1303.4157](#)].

- [14] M. J. Savage, *Phys. Lett.* **B331** (1994) 411–417, [[hep-ph/9404285](#)].
- [15] C. Garcia-Recio, J. Nieves, E. Ruiz Arriola, and M. Vicente Vacas, *Phys. Rev.* **D67** (2003) 076009, [[hep-ph/0210311](#)].
- [16] T. Sekihara, T. Hyodo, and D. Jido, *Phys. Rev.* **C83** (2011) 055202, [[arXiv:1012.3232](#)].
- [17] T. Hyodo and D. Jido, *Prog. Part. Nucl. Phys.* **67** (2012) 55–98, [[arXiv:1104.4474](#)].
- [18] M. Doring, U. Meißner, E. Oset, and A. Rusetsky, *Eur. Phys. J.* **A48** (2012) 114, [[arXiv:1205.4838](#)].
- [19] J. M. M. Hall, W. Kamleh, D. B. Leinweber, B. J. Menadue, B. J. Owen, A. W. Thomas, and R. D. Young, *PoS LATTICE2014* (2014) 094, [[arXiv:1411.0001](#)].
- [20] D. B. Leinweber, A. W. Thomas, and R. D. Young, *Phys. Rev. Lett.* **92** (2004) 242002, [[hep-lat/0302020](#)].
- [21] E. Veit, B. K. Jennings, R. Barrett, and A. W. Thomas, *Phys. Lett.* **B137** (1984) 415.
- [22] E. Veit, B. K. Jennings, A. W. Thomas, and R. Barrett, *Phys. Rev.* **D31** (1985) 1033.
- [23] **Particle Data Group** Collaboration, J. Beringer et al., *Phys. Rev.* **D86** (2012) 010001.
- [24] **PACS-CS Collaboration** Collaboration, S. Aoki et al., *Phys. Rev.* **D79** (2009) 034503, [[arXiv:0807.1661](#)].
- [25] L. S. Geng and E. Oset, *Eur. Phys. J.* **A34** (2007) 405–412, [[arXiv:0707.3343](#)].
- [26] V. K. Magas, E. Oset, and A. Ramos, *Phys. Rev. Lett.* **95** (2005) 052301, [[hep-ph/0503043](#)].
- [27] **Crystal Ball** Collaboration, S. Prakhov et al., *Phys. Rev.* **C70** (2004) 034605.
- [28] T. Hyodo, A. Hosaka, E. Oset, A. Ramos, and M. J. Vicente Vacas, *Phys. Rev.* **C68** (2003) 065203, [[nucl-th/0307005](#)].
- [29] T. Hyodo, A. Hosaka, M. J. Vicente Vacas, and E. Oset, *Phys. Lett.* **B593** (2004) 75–81, [[nucl-th/0401051](#)].
- [30] R. Molina and M. Doring, [arXiv:1512.0583](#).
- [31] R. A. Briceño and M. T. Hansen, [arXiv:1509.0850](#).